EBioMedicine 13 (2016) 212–224

Contents lists available at ScienceDirect

EBioMedicine

journal homepage: www.ebiomedicine.com

Research Paper

Progranulin Recruits HSP70 to β-Glucocerebrosidase and Is Therapeutic Against Gaucher Disease

Jinlong Jian [a], Qing-Yun Tian [a], Aubryanna Hettinghouse [a], Shuai Zhao [a], Helen Liu [a], Jianlu Wei [a], Gabriele Grunig [b], Wujuan Zhang [c], Kenneth D.R. Setchell [c], Ying Sun [d], Herman S. Overkleeft [e], Gerald L. Chan [f], Chuan-ju Liu [a,g,*]

[a] Department of Orthopaedic Surgery, New York University School of Medicine, New York, NY 10003, United States
[b] Department of Environmental Medicine, New York University School of Medicine, 57 Old Forge Road, Tuxedo, NY 10987, United States
[c] Division of Pathology, Cincinnati Children's Hospital Medical Center, Cincinnati, OH 45229, United States
[d] Division of Human Genetics, Cincinnati Children's Hospital Medical Center, Department of Pediatrics, University of Cincinnati College of Medicine, Cincinnati, OH 45229, United States
[e] Leiden Institute of Chemistry, Leiden University, Gorlaeus Laboratories, Einsteinweg 55, 2300 RA Leiden, The Netherlands
[f] Harvard T.H. Chan School of Public Health, 665 Huntington Avenue, Boston, MA 02115, United States
[g] Department of Cell Biology, New York University School of Medicine, New York, NY 10016, United States

ARTICLE INFO

Article history:
Received 22 August 2016
Received in revised form 3 October 2016
Accepted 7 October 2016
Available online 24 October 2016

Keywords:
Progranulin
HSP70
β-glucocerebrosidase
Gaucher disease
Lysosomal storage diseases
Pcgin

ABSTRACT

Gaucher disease (GD), the most common lysosomal storage disease, is caused by mutations in *GBA1* encoding of β-glucocerebrosidase (GCase). Recently it was reported that progranulin (PGRN) insufficiency and deficiency associated with GD in human and mice, respectively. However the underlying mechanisms remain unknown. Here we report that PGRN binds directly to GCase and its deficiency results in aggregation of GCase and its receptor LIMP2. Mass spectrometry approaches identified HSP70 as a GCase/LIMP2 complex-associated protein upon stress, with PGRN as an indispensable adaptor. Additionally, 98 amino acids of C-terminal PGRN, referred to as Pcgin, are required and sufficient for the binding to GCase and HSP70. Pcgin effectively ameliorates the disease phenotype in GD patient fibroblasts and animal models. These findings not only demonstrate that PGRN is a co-chaperone of HSP70 and plays an important role in GCase lysosomal localization, but may also provide new therapeutic interventions for lysosomal storage diseases, in particular GD.

1. Introduction

Gaucher disease (GD), a common lysosomal storage disease (LSD), is caused by mutations in *GBA1* with resultant defective glucocerebrosidase (GCase) function and the consequent accumulation of β-glucosylceramide (β-GlcCer) in macrophages and other cell types (Brady et al., 1965; Platt, 2014). β-GlcCer storage transforms lysosomes into tubular-like structures as viewed by electronic microscopy, with the lipid-engorged macrophage (Gaucher cell) showing a characteristic "wrinkled tissue paper" appearance under light microscopy. There are three types of GD based on its neurological complications (Beutler, 1991). Type 1 GD, the most common, is a non-neuropathic form occurring predominantly in patients of Ashkenazi Jewish descent; characteristics include hepatosplenomegaly, thrombocytopenia, anemia, osteonecrosis and sclerosis, diffuse osteopenia, and multiple osteologic complications (Beutler, 1991). Type 2 (or acute infantile neuropathic Gaucher's disease) begins within 6 months of birth and presents with serious convulsions, hypertonia, mental retardation and apnea. Children with Type 2 usually die before two years of age. Type 3 GD, a chronic neuropathic form, can begin at any time in childhood or even in adulthood. It is characterized by slowly progressive, milder neurologic symptoms as compared to acute type 2 GD.

Progranulin (PGRN), also known as granulin, epithelin precursor (GEP), PC-cell-derived growth factor (PCDGF), proepithelin, and acrogranin, contains seven-and-a-half repeats of a cysteine-rich motif (CX5–6CX5CCX8CCX6CCXDX2HCCPX4CX5–6C) and forms a unique "beads-on-a-string" structure (Hrabal et al., 1996). PGRN is abundantly expressed in epithelial cells, in chondrocytes, in cells of the immune system, and in neurons (Bateman and Bennett, 2009). PGRN is known to play a critical role in a variety of physiologic and disease processes, including early embryogenesis, wound healing (He et al., 2003), and host defense (Jian et al., 2013a). PGRN also functions as a neurotrophic factor and mutations in the PGRN gene (*GRN*) resulting in partial or complete loss of the PGRN protein were reported to associate with

* Corresponding author at: Rm 1608, HJD, New York University School of Medicine, 301 East 17th Street, New York, NY 10003, United States.
E-mail address: chuanju.liu@nyumc.org (C. Liu).

http://dx.doi.org/10.1016/j.ebiom.2016.10.010

frontotemporal dementia (FTD) (Baker et al., 2006; Cruts et al., 2006) and neuronal ceroid lipofuscinosis (NCL) (Ahmed et al., 2010; Gotzl et al., 2014), respectively.

PGRN associates with particular members in the TNF receptor superfamily, including TNFR1, TNFR2 and DR3 (Tang et al., 2011; Jian et al., 2013b; Liu et al., 2014; Li et al., 2014), and possesses the ability to suppress inflammation in various conditions (Zhu et al., 2002; Tang et al., 2011). Auto-antibodies against PGRN have been found in several autoimmune diseases, including rheumatoid arthritis, psoriatic arthritis, and inflammatory bowel disease, and such antibodies were shown to promote a proinflammatory environment in a subgroup of patients (Thurner et al., 2013; Thurner et al., 2014).

We recently reported that the four single nucleotide polymorphism (SNP) sites in *GRN*, the gene encoding PGRN, lead to PGRN insufficiency and have significantly higher frequency in GD patients; revealing an association between PGRN insufficiency and GD (Jian et al., 2016). In addition, "aged" and challenged adult PGRN null mice develop GD-like phenotypes (Jian et al., 2016). However, the mechanisms underlying the association between PGRN and GD remain unclear. In this study, we report that PGRN is a co-chaperone for the lysosomal localization of GCase under pathological conditions through linking GCase to heat shock protein 70 (HSP70), an evolutionarily highly conserved molecular chaperone that mediates folding and unlocks disaggregation of numerous proteins (Rothman and Schekman, 2011; Nillegoda et al., 2015; Nillegoda and Bukau, 2015; Matsuda et al., 2003; Parenti et al., 2015). More importantly, a 15-kDa PGRN-derived protein, referred to as Pcgin, effectively ameliorates the cellular phenotypes of GD.

2. Methods

2.1. Materials

Fibroblasts from Types 1 and 2 GD patients were purchased from Coriell Cell Repositories (Camden, NJ). Airway epithelial cells from WT and HSP70 KO mice were kindly provided by Dr. Lee (Zhang et al., 2016). Antibodies against GCase (sc-100544, sc-30844, and sc-32883), PGRN (SC-28928), Sortilin (sc-376576), α-GLA (sc-25823), HSP70 (sc-373867), Calregulin (sc-373863), TGN38 (sc-271624), EEA1 (sc-365652) LIMP2 (sc-55571), LAMP2 (sc-18822), His-tag (sc-803), GFP (sc-8334), and DsRed (sc-33353) were purchased from Santa Cruz Biotechnology (Dallas, Texas). Fluorescence labeled secondary antibodies were purchased from Jackson ImmunoResearch Laboratories, Inc. (West Grove, PA). Recombinant His-tag PGRN protein was purified from 293T stable cell lines as described previously (Feng et al., 2010; Tang et al., 2011). Recombinant GCase (Cat. No. 7410-GH-010), sortilin (Cat. No. 3154-ST-050), and LIMP2 (Cat. No. 1966-LM-050) proteins and sheep anti-mouse PGRN antibody (AF2557) were purchased from R&D Systems (Minneapolis, MN). ELISA kits to detect murine TNF-α, IL-1β, and IL-6 were purchased from eBioscience, Inc. (San Diego, CA).

2.2. Construction of Expression Plasmids

cDNAs encoding either full-length human PGRN or its serial N-terminal or C-terminal deletion mutants were cloned into pEGFP-N1 vectors by using *Eco*RI and *Bam*HI sites. The amino acid number encoded by C-terminal Deletions (CD) constructs: full-length PGRN (aa 1-593), CD1 (aa 1-521), CD2 (aa 1-444), CD3 (aa 1-376), CD4 (aa 1-284), CD5 (aa 1-209), CD6 (aa 1-127), and CD7 (aa 1-61). The amino acid number encoded by N-terminal Deletions (ND) constructs: ND1 (aa 45-593), ND2 (aa 113-593), ND3 (aa 179-593), ND4 (aa 261-593), ND5 (aa 336-593), ND6 (aa 416-593), and ND7 (aa 496-593). All constructs were confirmed by DNA sequence. Full-length human GCase was purchased from Addgene (Cambridge, MA) and subcloned to pDsRed-monomer N1 vector (Clontech Mountain View, CA). All constructs were confirmed by DNA sequencing.

2.3. Preparation of Lipid Extraction

Mouse brain tissue was used as a source of lipid mixture. Briefly, one mouse brain was dissected under sterile conditions. The brain tissues were homogenized in 50 ml DMEM medium containing 10% FBS. Bicinchoninic acid assay was used to determine the protein level in the brain lysate.

2.4. Expression and Purification of Pcgin

The sequence for Pcgin was inserted into pD444 expression vector with a His-tag (from DNA2.0, Menlo Park, CA). Pcgin was expressed in the BL21(DE3) *E. coli* strain after induction by 1 mM IPTG. After a 3 h culture, cells were pelleted and sonicated to release the fusion protein. His-tagged Pcgin was purified by using ProBond™ Purification System (Life Technology, Carlsbad, CA) as we have previously described (Tang et al., 2011). Briefly, supernatant of cell lysis was incubated with affinity beads overnight, and washed with washing buffer (50 mM NaH_2PO_4, 200 mM NaCl, 50 mM Imidazole, pH 8.0) six times. Pcgin was eluted from beads with elution buffer (50 mM NaH_2PO_4, 200 mM NaCl, 250 mM Imidazole, pH 8.0). After dialysis with PBS, endotoxin removal, and 0.2 μm filter sterilization, recombinant Pcgin protein was used in our cell-based model and in vivo animal model.

2.5. Site-directed Mutagenesis

pEGFP vector containing the Pcgin sequence was used as a template to create serial deletion mutants using a site-directed mutagenesis kit (Stratagene Ipswich, MA). Five deletion mutants were made to cover the full-length Pcgin: Δ1 delete aa496-522, Δ2 delete aa523-534, Δ3 delete aa535-539, Δ4 delete aa540-573 and Δ5 delete aa574-593. All mutant constructs were confirmed by DNA sequencing and their expressions were examined by western-blot.

2.6. Chronic Lung Inflammation Model

C57B/L6 WT and PGRN KO mice were housed in the animal facility of New York University as previously described (Tang et al., 2011). All animal experiments have been approved by Institutional Animal Care and use Committee (IACUC) of New York University School of Medicine. 8 week-old mice were induced with chronic lung inflammation by intraperitoneal (I·P.) injection of OVA-Alum at Day 1 and Day 15, followed by intranasal challenge with 1% OVA, beginning at Day 29 and administered at a frequency of every three days for the duration of four weeks (Daley et al., 2008).

To evaluate Pcgin's therapeutic function in vivo, a GD phenotype was induced in 8-week-old PGRN KO mice ($n = 10$) by OVA as described by above. One group of mice were injected with Pcgin (4 mg/kg/week) starting from the first week of intranasal challenge until to the end of this experiment and another group of mice were treated with Imiglucerase (60 u/kg/week) as a positive control. After 5 weeks of treatment with Pcgin or Imiglucerase, mice were sacrificed and lung tissues were fixed and processed by Mass Histology Service (Worcester, MA).

2.7. Right Ventricular Systolic Pressure (RVSP)

The right jugular veins of anesthetized WT and PGRN KO mice were exposed under an anatomic microscope. The RVSP was measured as reported previously (Park et al., 2015). Briefly, a catheter was inserted into right ventricular chamber via the jugular vein and RVSP was measured. Mice were analyzed without prior knowledge of group identity. The data from three independent experiments were pooled.

2.8. Histology and Analysis

After mice were sacrificed, lung tissues were embedded in paraffin, cut into slides, and stained with H&E and PAS by Mass Histology Service (Worcester, MA). Quantification of Gaucher cell count and measurement of area occupied by Gaucher cells was analyzed by Image J software.

2.9. Transmission Electron Microscope (TEM)

WT and PGRN KO mice after OVA treatment were anesthetized and the lung was processed for TEM or immunogold EM staining at microscope core facility at New York University School of Medicine (Jian et al., 2016). Briefly, mice were euthanized and the lung was perfused with fixative containing 2.5% Glutaraldehyde and 2% paraformaldehyde in 0.1 M sodium cacodylate buffer (pH 7.2) for 2 h. The samples were post fixed in 1% OsO4 for 1 h, block stained with 1% uranyl acetate, dehydrated and embedded in Embed 812 (Electron Microscopy Sciences, Hatfield, PA). 60 nm sections were cut, and stained with uranyl acetate and lead citrate by standard methods. Stained grids were examined under Philips CM-12 electron microscope (FEI; Eindhoven, The Netherlands) and photographed with a Gatan (4 k × 2.7 k) digital camera (Gatan, Inc., Pleasanton, CA).

For immunoelectron microscopy, lungs were fixed with 4% PFA in 0.1 M phosphate buffer (pH 7.4). The tissues were embedded in Lowicryl K4M (Polysciences, Inc.,Warrington, PA) and LR White (Electron Microscopy Sciences, Hatfield, PA). Polymerization was carried out under UV light (360 nm) at −35 °C for LK4M and −10 °C for LR White. After incubation with primary antibodies at 4 °C overnight, gold conjugated secondary antibodies (15 nm Protein A Gold, Cell Microscopy Center, University Medical Center Utrecht, 35584 CX Utrecht, The Netherlands; 18 nm Colloidal Gold-AffiniPure Goat Anti-Rabbit IgG (H + L), Jackson ImmunoReasearch Laboratories, Inc., West Grove, PA) were applied.

For double immunogold labeling, the tissue sections were incubated with mouse antibodies against GBA, or HSP70, followed by incubation with secondary antibody labeled with 5 nm gold particle. Then the sections were incubated with rabbit anti-PGRN antibody, followed by incubation with secondary antibody labeled with 18 nm gold particle. The grids were stained and examined as described above.

2.10. Surface Plasmon Resonance (SPR)

Binding affinity between GCase and PGRN were measured by SPR experiments by SensiQ Technologies Inc. (Oklahoma City, OK) as previously described (Tang et al., 2011; Jian et al., 2013b).

2.11. Fluorescence Resonance Energy Transfer (FRET)

293 EBNA cells in 96-well plates were transfected with pDsRed-GBA and pEGFP-PGRN·Cells transfected with pDsRed empty vector were employed as baseline control. The fluorescence intensity was read by SpectraMax® i3x Platform from Molecular Devices (Sunnyvale, CA). The cells were excited by GFP excitation wavelength (488 nm) and detect the DsRed emission wavelength (588 nm).

2.12. Immunofluorescence Staining and Confocal Microscope

Frozen lung sections, or cover-slip cultured cells, were fixed with 4% formaldehyde and permeabilized by 0.1% Triton-100 PBS. Primary antibodies were probed at 4 °C degree overnight, followed by fluorescence-labeled secondary antibodies. The tissues or cultured cells were mounted on anti-fade medium containing DAPI. The images were taken by Leica TCS SP5 con-focal system.

2.13. Immunoprecipitation

Lungs from WT and PGRN KO mice with or without OVA challenge, or in another experiment from control PGRN KO mice, or OVA-challenged PGRN KO mice with or without rPGRN treatment, were lysed with RIPA lysis buffer containing protease inhibitors. The same amount of proteins from each group of mice was mixed together to represent the protein profile of each group. 400 μg protein from mixed samples were used for immunoprecipitation.

To determine the interaction between PGRN and GCase in cells, 293 EBNA cells were co-transfected with plasmids encoding Flag-tagged PGRN and RFP-fused GCase. Cells were collected by RIPA buffer, lysates were immunoprecipitated with anti-Flag antibody, and the protein complexes were detected with anti-GCase antibody.

To dissect the domains of PGRN responsible for binding to GCase, 293 EBNA cells were transfected with the plasmids encoding GFP fused full-length PGRN, or its serial deletion mutants, together with an expression plasmid encoding RFP fused GCase. 48 h after transfection, the cells were lysed and samples were processed as described above.

All the samples were incubated overnight with primary antibodies and protein A/G agarose-beads, followed by thorough washing with RIPA lysis buffer. The samples were run on SDS-PAGE. Targeted proteins were probed with antibody and visualized by western-blot. In some experiments, the samples were sent to NYU Core Facility for Mass Spectrometry after immunoprecipitation.

2.14. Mass Spectrum

1) Gel Separation and Digestion. Samples were reduced with DTT at 57 °C for 1 h and were alkylated with Iodoacetamide for 45 min. Each sample was loaded onto a NuPAGE® 4–12% Bis-Tris Gel 1.0 mm The gel was stained using GelCode Blue Stain Reagent (Thermo Scientific) and Coomassie stained gel bands were excised as indicated on the gel image. Excised gel pieces were destained with a 50:50 *v*/v solution of methanol and 100 mM ammonium bicarbonate. 300 ng of trypsin (Promega) were added to digest the gel pieces. 2) Protein Extraction. A slurry of R2 20 μm Poros beads (Life Technologies Corporation) in 5% formic acid and 0.2% trifluoroacetic acid (TFA) was added to each sample. The samples were shaken at 4 °C for 2 h. The beads were loaded onto equilibrated C18 ziptips (Millipore) using a microcentrifuge for 30 s at 6000 rpm. Gel pieces were rinsed three times with 0.1% TFA. The extracted porors beads were further washed with 0.5% acetic acid. Peptides were eluted by the addition of 40% acetonitrile in 0.5% acetic acid followed by the addition of 80% acetonitrile in 0.5% acetic acid. The organic solvent was removed using a SpeedVac concentrator and the sample reconstituted in 0.5% acetic acid. 3) MS Analysis. 1/5th of each sample was analyzed individually with the mIgG analyzed first, then the KO GBA, and finally the WT GBA. Samples were injected for on-line LC-MS using the autosampler of a EASY-nLC 1000 (Thermo Scientific). Peptides were gradient eluted from the column directly to Q Exactive mass spectrometer (Thermo Scientific) using a 1 h gradient Solvent A: 5% acetonitrile, 0.5% acetic acid Solvent B: 95% acetonitrile, 0.5% acetic acid. 4) MS Method. High resolution full MS spectra were acquired with a resolution of 70,000, an AGC target of 1e6, with a maximum ion time of 120 ms, and scan range of 300 to 1500 *m*/*z*. Following each full MS twenty data-dependent high resolution HCD MS/MS spectra were acquired. All MS/MS spectra were collected using the following instrument parameters: resolution of 17,000, AGC target of 2e5, maximum ion time of 250 ms, one microscan, 2 *m*/*z* isolation window, fixed first mass of 150 m/z, and NCE of 27. MS/MS spectra were searched against a UniProt mouse database using Sequest within Proteome Discoverer.

2.15. Immunohistochemistry

Paraffin-embedded lung slides from WT and PGRN KO mice were deparaffined in a xylene and ethanol gradient. After antigen retrieval by 0.1% trypsin and inactivation of endogenous hydrogen peroxidase, the slides were blocked with 3% BSA and 20% goat serum for 30 min. Primary antibodies were diluted at 1:20–50 with 2% goat serum and primed on the slides at 4 °C overnight. The next day, slides were washed with PBS and secondary antibodies were added (1:200 biotin-labeled goat-anti rabbit antibody or goat-anti mouse antibody) for 1 h. The staining was visualized by Vector ABC peroxidase kit, followed by DAB substrates.

2.16. Fluorescence Labeling of Active Form of GCase

MDW933, a specific ultrasensitive fluorescent dye for active lysosomal GCase (Witte et al., 2010; Gaspar et al., 2014), was a kindly provided by Dr. Hermen E. Overkleeft at University of Leiden. Cells were cultured on cover glass, and MDW933 (50 nM) was added in cell culture medium for 2 h to label lysosomal GCase. Next, cells were fixed with 3% (v/v) paraformaldehyde in PBS for 15 min, permeabilized by 0.1 mM NH4Cl in PBS for 10 min, Cells were mounted with DAPI-medium, and fluorescence was visualized under a confocal microscope.

2.17. Knockdown of PGRN and HSP70 by siRNA

siRNA against mouse PGRN and HSP70 were purchased from Life Technology. 20 pmol of each siRNA were transiently transfected into RAW264.7 cells by Lipofectamine 2000. The cells were treated with lipid mixture (50 μg/ml) for 24 h and the level of the active form of GCase was measured by MDW933 dye. The knockdown of PGRN or HSP70 was confirmed by immunofluorescence staining using their specific antibodies.

2.18. Lysosome Staining in LSD Fibroblasts

Fibroblasts from GD patients were cultured on coverslips in 24-well plates, and challenged with lipid lysis (50 μg/ml), with PGRN (0.4 μg/ml) or Pcgin (5 μg/ml) for 24 h. The next day, fresh medium containing 100 nM LysoTracker® Red was added for 1 h. The cells were washed with PBS and fixed in 2% PFA. The coverslips were mounted on slides and the staining of lysosomes was imaged by confocal microscopy. Ten images were randomly taken from each sample, and fluorescence intensities were measured by ImageJ software.

2.19. Lysosome Staining by Live Imaging System

Full-length PGRN, as well as its serial deletion mutants, was cloned into pEGFP vector, and transiently transfected into GD fibroblasts seeded in Lab-Tek Chamber cover glass system. After 48 h in culture, LysoTracker® Deep Red (50 nM) was added to the medium for 1 h. The LysoTracker Deep Red signaling (excitation/emission of 647/668 nm) was observed in live cells by Applied Precision Personal DV live-cell imaging system at NYU core facility.

GFP + positive cells indicated the expression of PGRN or its mutants, and GFP − negative cells were un-transfected control cells. The therapeutic effect of PGRN, as well as its mutants, was evaluated by comparing the LysoTracker signal between GFP + and GFP − cells. Ten images were taken for each sample, and fluorescence intensity of lysosome of GFP + and GFP − cells were selected and quantified by ImageJ.

2.20. GlcCer Quantitation

GlcCer contents in cell and spleen were quantitated by LC/MS following glycosphingolipids extraction as described (Sun et al., 2005). Internal standard of D_5-C18-GlcCer was added prior to extraction. LC/MS was carried out on a Waters Quattro Premier XE triple quadruple mass spectrometer interfaced with Aquity UPLC system (Milford, MA). GlcCer were quantified using 3 GlcCer reference standards (C16, C18 and C24-1 GlcCer) based on multiple reaction monitoring (MRM) function on mass spectrometer. Quantification of GlcCer with various chain lengths was accomplished using the curve for the GlcCer of closest chain length. Total GlcCer was the sum of individual GlcCer species detected. The GlcCer levels were normalized by protein amount in the cells and by tissue weight in spleen.

2.21. Statistical Analysis

For comparison of treatment groups, we performed unpaired *t*-tests, paired *t*-tests, and one-way or two-way ANOVA (where appropriate). All statistical analysis was performed using SPSS Software. Statistical significance was two-sided and was achieved when at $p < 0.05$.

3. Results

3.1. PGRN is Required for GCase Lysosomal Appearance and Its Deficiency Causes GCase/LIMP2 Aggregation

The findings that PGRN plays important anti-inflammatory and immunoregulatory roles in various conditions, including inflammatory arthritis (Tang et al., 2011), prompted us to examine its involvement in chronic lung inflammation. For this purpose, chronic lung inflammation was induced in 8-week old WT and PGRN knockout (KO) mice by intraperitoneal (IP) injection of ovalbumin (OVA) at Day 1 and 15, followed by intranasal challenge of 1% OVA three times a week for four weeks beginning at Day 29. PGRN expression was induced in WT mice after OVA challenge (Fig. S1a), and PGRN KO mice developed more severe lung inflammation, including increased levels of inflammatory cytokines, pulmonary cell infiltration, and right ventricular systolic pressure (Fig. S1b–f). Remarkably, large numbers of "giant cells" were found in the lungs of PGRN KO mice, particularly after OVA treatment (Fig. 1a). These cells were engorged with materials and had a "wrinkled tissue paper" appearance, which is the typical morphology of Gaucher cells. No such cells were found in WT mice, either with or without OVA challenge. The liver and spleen were larger in PGRN KO mice relative to those in WT mice (Fig. 1b). In accordance with our previous report that β-GlcCer is accumulated in the lung tissue of PGRN KO mice, lipid composition analysis revealed that GlcCer (Jian et al., 2016), as well as levels of GlcSph (glucosylsphingosine), were significantly higher in both lung and plasma of PGRN KO mice as compared to WT mice (Fig. S2). These macrophages from PGRN KO mice were much larger than those in WT mice, and the PGRN KO lysosome displayed the classic Gaucher-like cell tubular shape, instead of a regular round shape, as viewed under transmission electronic microscope (TEM) (Fig. 1c). The transformation of lysosome from the normal round shape to a tubular-like structure was observed along with material accumulation (Fig. S3). Other organelles, such as mitochondria and endoplasmic reticulum, and other types of cells, such as type 1 and 2 pneumocyte, appeared normal (Figs. S4, S5), although defects in mitochondrial function have been reported in GD (Gegg and Schapira, 2016; de la Mata et al., 2015). The tubular-like structure was confirmed as lysosome through immunogold EM staining with the lysosomal receptor Sortilin (Figs. S6).

Accumulation of β-GlcCer in GD is caused by reduced GCase enzymatic activity or decreased GCase protein expression (Grabowski, 2012). However the protein level and GCase enzymatic activity were not affected in PGRN KO mice (Jian et al., 2016). Immunohistochemistry staining of GCase revealed that intracellular localization of GCase was dramatically altered. Remarkably, GCase was aggregated in the cytoplasm in OVA-challenged PGRN KO mice (Fig. 1d). Immunogold labeling TEM further demonstrated that GCase was aggregated in PGRN null macrophages (Fig. 1e). The specificity of GCase antibody was examined with *Gba1* −/− tissues (Fig. S7). As a control for the immunogold labeling TEM, Sortilin was found mainly to be clustered close to the cell plasma

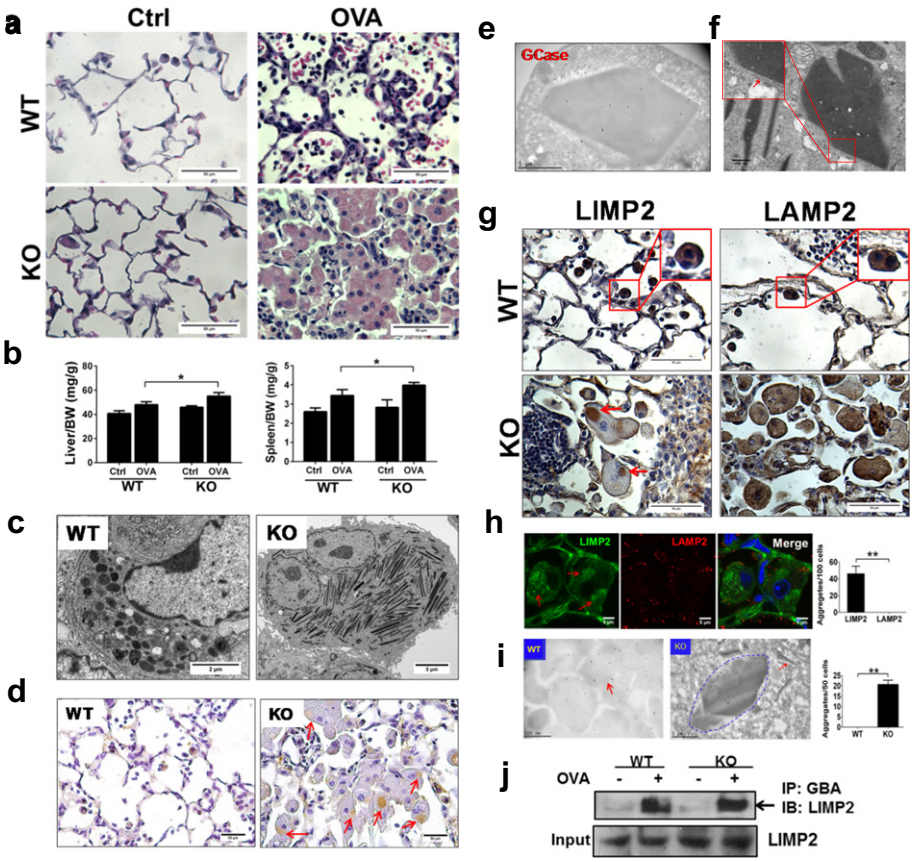

Fig. 1. PGRN is required for GCase lysosomal appearance and its deficiency causes GCase/LIMP2 aggregation. WT and PGRN KO mice received I.P. injection of OVA at Day 1 and 15, followed by intranasal challenge of 1% OVA beginning at Day 29 and administered thereafter three times a week for four weeks. (a) H&E staining shows giant Gaucher-like cells in lung of both male and female PGRN KO mice, especially after OVA treatment. (n = 10, 5 male and 5 female for each group). (b) Spleen and liver are larger in OVA-challenged PGRN KO mice than in WT mice (n = 10, 5 male and 5 female for each group). (c) Macrophages from PGRN KO mice are much larger than those in WT mice, and lysosomes become a tubular-like shape instead of the regular round shape, as assayed by transmission electronic microscope (TEM). (d) Distribution of GCase is altered in PGRN KO macrophages. Paraffin-embedded lung slides from OVA-challenged mice were stained with GCase antibody by immunohistochemistry. The aggregation of GCase in PGRN KO macrophages is indicated with arrows. (e) GCase is aggregated in the cytoplasm in of PGRN null macrophage, assayed by immunogold labeling of lung tissue. (f) The membrane of the aggregation structure in PGRN KO mice under EM. Lung tissues from PGRN KO mice after OVA challenge were processed for EM scanning. The membrane structure around aggregates is indicated by the red arrow. (g) Expression of LIMP2 and LAMP2 in macrophages from OVA-challenged WT and PGRN KO mice. Paraffin-embedded lung slides from WT and PGRN KO mice were stained with LIMP2 and LAMP2 by immunohistochemistry. Aggregation of LIMP2 in PGRN KO macrophages was indicated with an arrow. (h) LIMP2, but not LAMP2, is aggregated in the cytoplasm of PGRN null macrophage, assayed by immunofluorescence staining. Frozen sections of lung tissue from OVA-challenged PGRN KO mice were stained with LIMP2 or LAMP2 antibodies by immunofluorescence. The aggregation of LIMP2 is indicated with an arrow. The numbers of LIMP2 aggregates and Gaucher-like cells were counted and indicated as aggregates/100 Gaucher-like cells (right panel). (i) LIMP2 is not detectable in the lysosome and is aggregated in the cytoplasm in the PGRN null macrophage, assayed by immunogold labeling of lung tissue. LIMP2 is detectable in the lysosome, indicated with an arrow, of WT macrophage (left panel, 53,000×), whereas it is aggregated in the cytoplasm of PGRN-null macrophage and not observed in the tubular-like lysosome (middle panel 31,000×). An aggregation region of denser immunogold labeling is circled with a dashed line. The numbers of aggregates of LIMP2 and Gaucher-like cells were counted and indicated as aggregates/50 Gaucher-like cells (right panel). (j) GCase binds to LIMP2 in the absence of PGRN in vivo, assayed by co-immunoprecipitation (Co-IP). Lung tissue from both WT and PGRN KO mice were lysed and protein complexes were immunoprecipitated with anti-GCase antibody and detected with anti-LIMP2 antibody.

membrane, mediating endocytosis, and was also present in the tubular-like lysosomes of Gaucher cells in PGRN KO mice (Fig. S6). TEM revealed that the aggregation of GCase was environed, at least partially, in/on a membrane structure (Fig. 1f). We also performed co-immunogold staining of GCase with various organelle markers, including ER, trans-Golgi network, lysosome, and autophagy markers. Intriguingly, GCase was found to be specifically co-localized with the autophagy marker LC3 in aggregates (Fig. S8). Taken together, these results demonstrate that the lysosomal localization of GCase depends on the presence of PGRN.

Lysosomal integral membrane protein 2 (LIMP2), known as a GCase-binding receptor that mediates delivery of GCase to lysosomes, is present in several subcellular organelles in the secretory pathway, including the lysosome (Reczek et al., 2007). Interestingly, we found that lysosomal localization of LIMP2 was also defective in OVA-challenged PGRN-deficient macrophages (Fig. 1g, h). However, intracellular localization of lysosomal associated membrane protein-2 (LAMP-2), a lysosomal marker, was not affected in OVA-challenged PGRN null macrophages. Specifically, both LIMP2 and LAMP2 were detected in the lysosomes of WT macrophages; however LIMP2 was aggregated, while LAMP2 was distributed normally, in PGRN null macrophages (Fig. 1g). Confocal staining with frozen sections of lung tissues also demonstrated the aggregation of LIMP2, but not LAMP2, in OVA-challenged (Fig. 1h) and aged (Fig. S9) PGRN deficient tissues. The cytoplasmic aggregation of LIMP2 was further confirmed with immunogold TEM staining (Fig. 1i). In addition, GCase and LIMP2 still bind together in both WT and PGRN KO tissues mice, as assayed by co-immunoprecipitation (Fig. 1j) and con-focal staining (Fig. S10), which is in accordance with the previous reports that indicating that sorting of GCase and LIMP2 are tightly linked (Reczek et al., 2007). Collectively, both GCase and its receptor LIMP2 were aggregated and absent from lysosomes in stressed (OVA-challenged or lipid-stimulated) PGRN deficient macrophages and mice.

3.2. PGRN Directly Binds to GCase Through a Two-site Mechanism

The finding that PGRN was required for lysosomal localization of GCase prompted us to determine whether PGRN directly associates

with GCase. In vivo interaction between PGRN and GCase was demonstrated by co-immunoprecipitation with both transfected cells (Fig. 2a) and native tissues from WT mice (Fig. 2b). TNFR2 was employed as a positive control for binding to PGRN (Tang et al., 2011; Jian et al., 2013b). We also determined whether PGRN directly binds to GCase using a solid-phase binding assay with recombinant PGRN and GCase. PGRN demonstrated dose-dependent binding and saturation to liquid-phase GCase (Fig. 2c), whereas no direct interaction between PGRN and LIMP2 was detected (Fig. 2c). The binding affinity between PGRN and GCase was then measured using surface plasmon resonance (SPR) with SensiQ Pioneer as described (Tang et al., 2011; Jian et al., 2013b). The results demonstrated that PGRN binds to GCase in a two-site model: The first binding site exhibited a very high binding affinity ($K_{D1} = 0.71$ nM), whereas the second one displayed a relatively weaker binding affinity ($K_{D2} = 360$ nM), at pH 7.4 (Fig. 2d). Intriguingly, these two binding sites responded differently to pH changes: The affinity for the high binding site decreased, whereas affinity for the weaker binding site increased, during pH reduction in the traffic process from endoplasmic reticulum (ER), Golgi, and trans-Golgi network (TGN) of macrophages (Fig. 2d, e), although GCase and PGRN co-localized in all of these intracellular traffic compartments, as revealed by immunofluorescence staining (Fig. S11). Double labeling immunogold TEM also showed that PGRN co-localized with GCase in the ER and lysosome (Fig. 2f). Taken together, these results suggest that the probable points of GCase and PGRN association are in the intracellular compartments, beginning in compartments as early as the ER.

To identify the domains of PGRN required for interacting with GCase, serial N-terminal deletions of PGRN were subcloned into pEGFP vector and the expressions of these GFP fused deletion mutants of PGRN were visualized with anti-GFP antibody (Fig. 3a, b). Co-IP was performed to examine the binding activities of these mutants to RFP-fused GCase encoded by the pDsRed-GCase plasmid (Fig. 3c). Deletion of Grn P and Grn G did not affect, whereas deletion of Grn F abolished, the interaction of PGRN with GCase, indicating that Grn F of PGRN is involved in the association between PGRN and GCase. Interestingly, further removal of Grn B resulted in a weak recovery of interaction, suggesting that Grn B might act as an inhibitory and regulatory domain for binding to GCase. Further deletions demonstrated that Grn E alone strongly bound to GCase (Fig. 3c). The binding pattern of these N-terminal deletion mutants of PGRN with GCase was also confirmed by fluorescence resonance energy transfer (FRET) assay (Fig. 3d). Indeed, the importance of the major and strong binding site Grn E in mediating the binding of PGRN to GCase was further demonstrated with serial C-terminal deletions of PGRN, since deletion of Grn E from C-terminus abolished the interaction in both Co-IP and FRET assays (Fig. 3e–h). Collectively, these sets of assays indicate that Grn E and F are the strong and weak binding sites, respectively, which also supports the aforementioned two-site binding mechanism of PGRN to GCase, first observed in our surface plasmon resonance (SPR) assay (Fig. 2d, e).

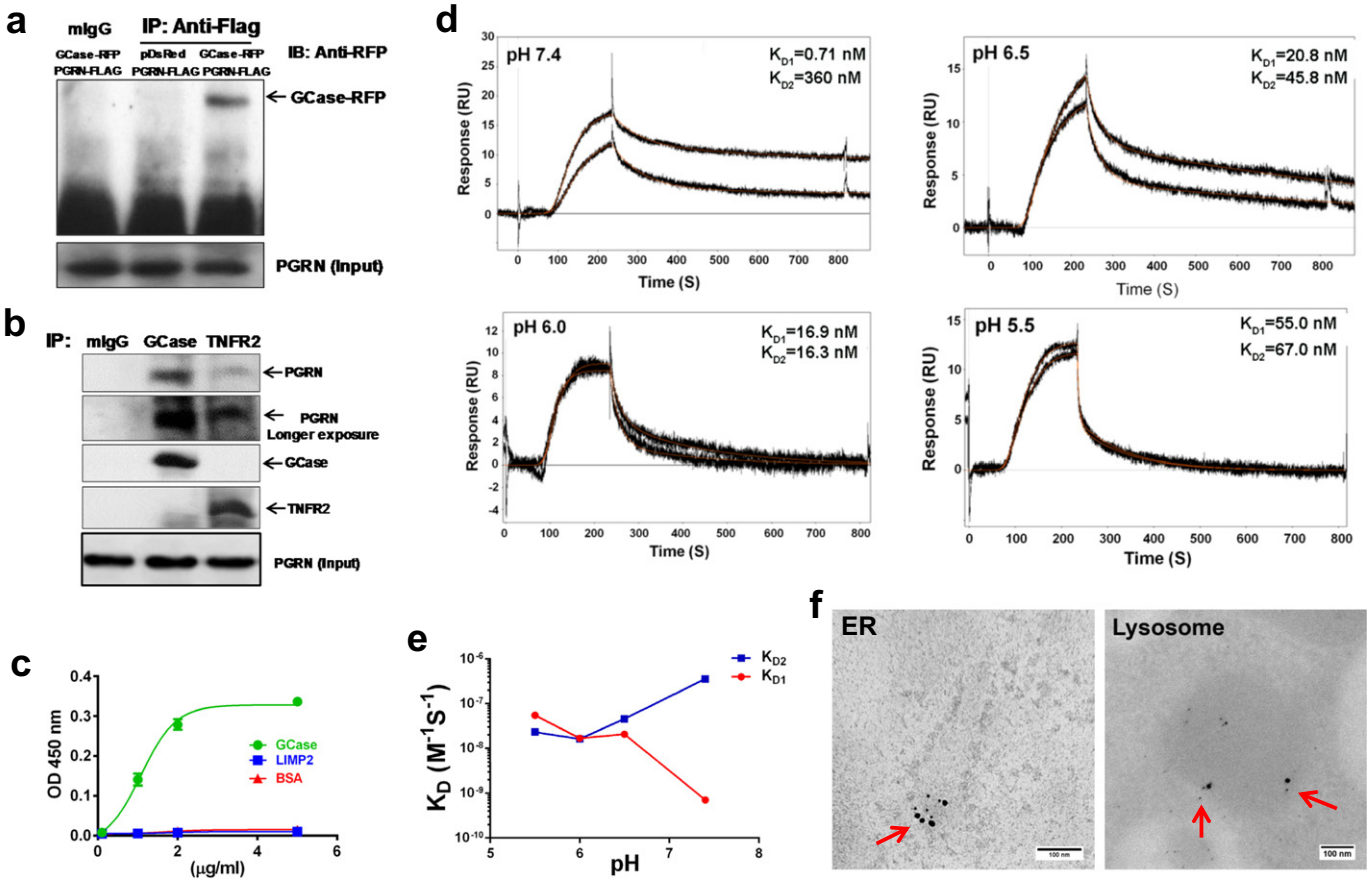

Fig. 2. PGRN directly binds to GCase in a two-sites binding mechanism. (a) PGRN binds to GCase in 293 EBNA cells transfected with plasmids encoding Flag-tagged PGRN and RFP-tagged GCase, assayed by co-immunoprecipitation (Co-IP). The cell lysates were immunoprecipitated by anti-Flag antibody and probed with RFP antibody. The result is representative of three independent experiments. (b) PGRN binds to GCase assayed by Co-IP. Lung tissues from WT mice were lysed and protein complexes were immunoprecipitated with anti-GCase or TNFR2 (serving as a positive control) antibody, and probed with anti-PGRN antibody. (c) PGRN directly binds to GCase in vitro, assayed by solid phase binding assay. Various amounts of PGRN were coated, and biotin-labeled BSA, LIMP2 and GCase were added, followed by HRP-labeled Streptavidin and its substrates. (d) PGRN binds to GCase in a two-site mechanism, and the binding affinity responds differently to decreasing pH in traffic, assayed by surface plasmon resonance (SPR) with COOH1 chips. (e) Effect of assay pH on kinetic binding values of both high and low affinity binding sites. (f) PGRN co-localizes with GCase in ER and lysosome in the macrophage, assayed by double immunogold labeling of lung tissue in WT mice. PGRN is labeled with 18 nm gold particle (large) and GCase is labeled with 5 nm gold particle (small), co-localizations are indicated by arrows.

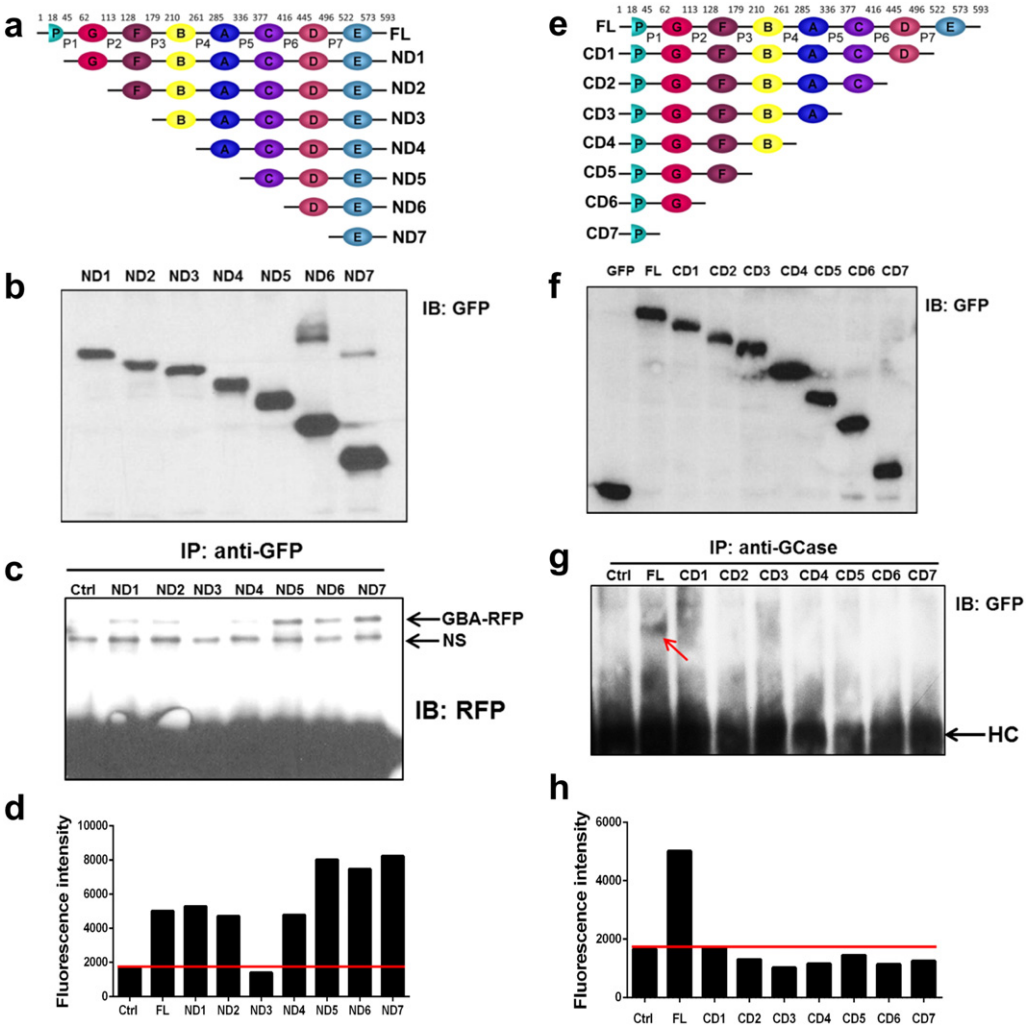

Fig. 3. PGRN binds to GCase through Grn E and Grn F. (a) Scheme of constructs encoding serial GFP-tagged N-terminal deletion mutants of PGRN. ND1 (aa 45-593), ND2 (aa 113-593), ND3 (aa 179-593), ND4 (aa 261-593), ND5 (aa 336-593), ND6 (aa 416-593), and ND7 (aa 496-593). (b) Expressions of GFP-tagged N-terminal deletion PGRN fragments, examined by immunoblotting with anti-GFP antibody. (c) Co-IP assay. 293 EBNA cells were transfected with pDsRed-GCase encoding RFP-fused GCase and corresponding plasmids encoding various GFP-fused N-terminal deletions of PGRN, as indicated, and the cell lysates were immunoprecipitated with GFP antibody. The complexes were probed with anti-RFP antibody. Control IgG (Ctrl) used as a negative control. NS indicates nonspecific binding. (d) FRET assay. 293 EBNA cells were transfected as described in (c), and the culture plate was scanned by SpectraMax® i3x Platform with GFP excitation wavelength (488 nm) and DsRed emission wavelength (588 nm). (e) Scheme of constructs encoding serial GFP-tagged C-terminal deletion mutants of PGRN. PGRN full-length (aa 1-593), CD1 (aa 1-521), CD2 (aa 1-444), CD3 (aa 1-376), CD4 (aa 1-284), CD5 (aa 1-209), CD6 (aa 1-127), and CD7 (aa 1-61). (f) Expressions of GFP-tagged C-terminal deletion PGRN fragments, examined by immunoblotting with anti-GFP antibody. (g) Co-IP assay. 293 EBNA cells were transfected with pDsRed-GCase encoding RFP-fused GCase and corresponding plasmids encoding various GFP-fused C-terminal deletions of PGRN, as indicated, and the cell lysates were immunoprecipitated with GCase BA antibody. The complexes were probed with anti-GFP antibody. The positive band is indicated with an arrow. HC indicates IgG heavy chain. (h) FRET assay. 293 EBNA cells were transfected as described in (g), and the culture plate was scanned by SpectraMax® i3x Platform with GFP excitation wavelength (488 nm) and DsRed emission wavelength (588 nm).

3.3. PGRN Recruits HSP70 to GCase/LIMP2 Upon Stress

We next sought to further determine the molecular mechanism by which PGRN deficiency leads to the aggregation of GCase. To isolate the molecules that are involved in PGRN's regulation of GCase, immunoprecipitation was performed with anti-GCase antibody from OVA-challenged WT and PGRN KO tissues, followed by mass spectrometry (MS). Immunoprecipitation with GCase antibody pulled-down both PGRN-dependent and PGRN–independent GCase-associated proteins in WT tissues. When the same immunoprecipitation experiment was performed in PGRN KO tissues, only PGRN-independent GCase-associated proteins were immunoprecipitated. Hits from WT mice were subtracted by hits from PGRN KO, to yield PGRN-dependent GCase associated proteins, with the rationale that the molecules involved in PGRN-mediated GCase localization would be among the hits only present in WT mice but not PGRN KO mice (Fig. 4a). 134 hits in WT mice and 114 hits in PGRN KO mice were identified. 95 of them were common in both groups, and 39 proteins were found to be specific for WT mice, suggesting that these proteins would be PGRN-dependent GCase-associated proteins (Fig. 4b). Perlecan and Leukocyte elastase inhibitor, two known PGRN-binding proteins (Zhu et al., 2002; Gonzalez et al., 2003), were identified among the 39 hits, validating the technique. In addition, HSP70 and its co-chaperone protein T-complex protein 1 subunit alpha (TCP1), as well as cytoskeleton, vesicle-traffic related proteins, and an energy producing enzyme, were among the 39 hits (Table S1). These data were followed up with the studies in HEK293EBNA cells stably transfected with an expression plasmid encoding His-tagged PGRN (Tang et al., 2011). Two proteins were co-purified with His-tagged PGRN, and MS analysis revealed that these were HSP70 and TCP1 (data not shown). To confirm the MS data, we conducted immunoprecipitation using an anti-GCase antibody in WT and PGRN KO tissues, and probed with an antibody against HSP70. HSP70 bound to GCase in WT mice after OVA challenge, and this interaction was undetectable in PGRN KO mice

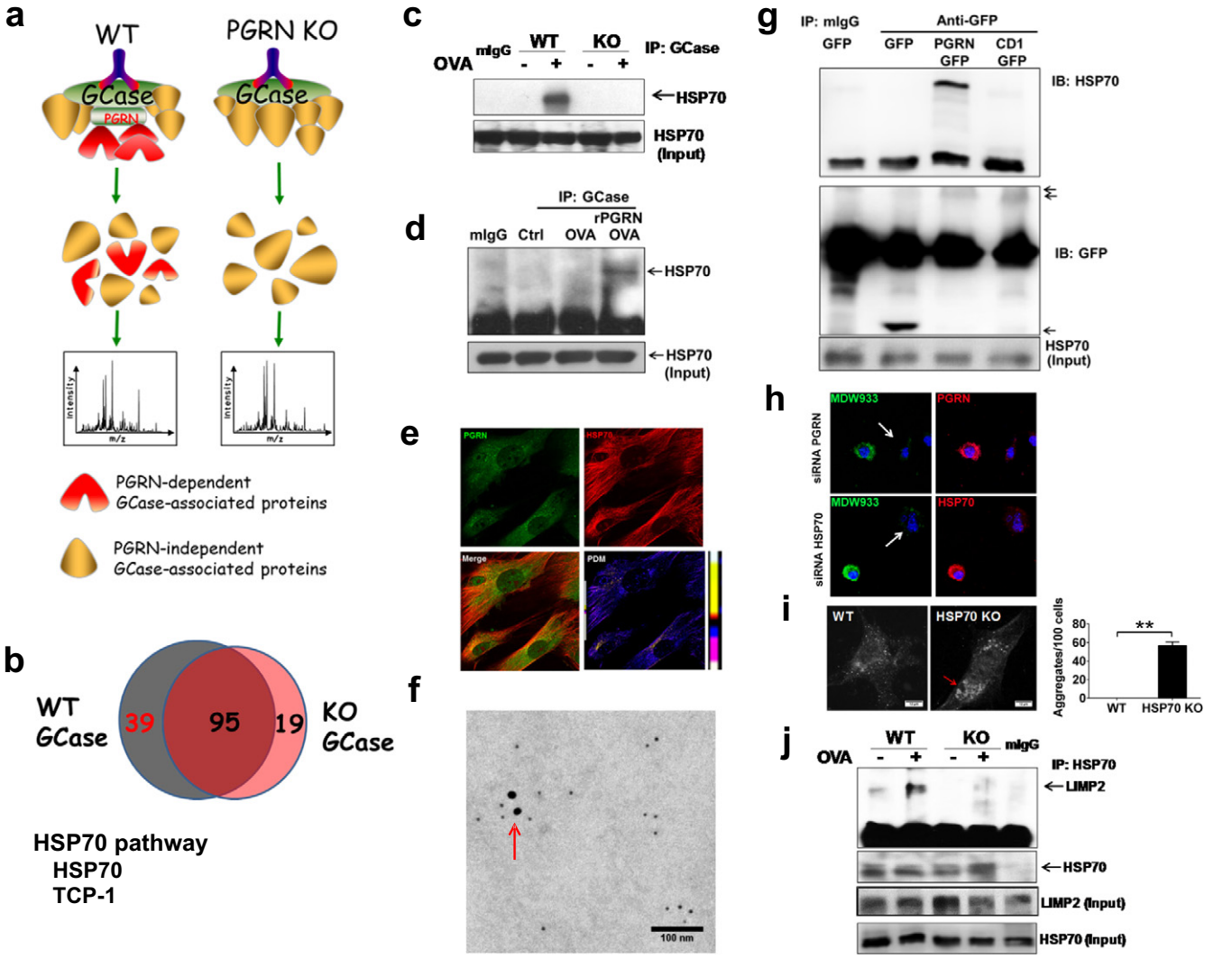

Fig. 4. Stress-induced PGRN-dependent interaction between GCase and HSP70. (a) The scheme of the method used to identify potential molecules involved in PGRN-mediated regulation of GCase, i.e. PGRN-dependent GCase associated proteins. Immunoprecipitation was performed with GCase antibody from both OVA-challenged WT and PGRN KO mice, followed by high-sensitivity mass spectrometry. (b) Summary of the hits isolated from both WT and PGRN KO mice and identification of HSP70 as a PGRN-dependent GCase-associated chaperone. (c) Binding of GCase to HSP70 is PGRN-dependent. Immunoprecipitation was conducted with anti-GCase antibody in WT and PGRN KO mice, and probed with HSP70 antibody. The result is representative of three independent experiments. (d) rPGRN restores the interaction between GCase and HSP70 in PGRN deficient mice in vivo. Lung tissue lysates prepared from OVA-unchallenged (Ctrl) or OVA-challenged PGRN KO mice treated with or without rPGRN were immunoprecipitated with anti-GCase antibody, and the presence of HSP70 in the immunoprecipitated complex was probed with HSP70 antibody. The result is representative of three independent experiments. (e) PGRN is co-localized with HSP70 in macrophages. Distribution of PGRN and HSP70 in BMDM were stained by the specific antibodies followed by fluorescence secondary antibodies, the co-localization is quantified as PDM Value (Product of the Differences from the Mean) shown in the lower right panel. (f) PGRN is co-localized with HSP70 in cytosol of macrophage, assayed by double immunogold labeling TEM of lung tissue in WT mice. PGRN is labeled with 18 nm gold particle (large) and HSP70 is labeled with 5 nm gold particle (small), and the co-localizations are indicated by arrow. (g) GrnE of PGRN is required for its binding to HSP70. A plasmid encoding GFP alone, GFP fused PGRN (FL) or C-terminal deletion of GrnE (CD1) mutation, was transfected into 293T cells. The interaction between PGRN and HSP70 were measured by immunoprecipitation with anti-GFP antibody and detected with HSP70 antibody. The result is representative of three independent experiments. (h) Suppression of PGRN and HSP70 via a siRNA approach markedly reduces the lysosomal GCase in living macrophage, assayed by MDW933 labeling. RAW264.7 macrophages were transfected with siRNA specifically against PGRN or HSP70. Cells pre-treated with lipid stimulation were labeled with MDW933 probe for 2 h, and the expression levels of PGRN and HSP70 were measured by immunofluorescence staining. The cell transfected with corresponding siRNA is indicated with an arrow. (i) GCase is aggregated in HSP70 deficient cells, assayed by immunofluorescence staining. Murine lung endothelial cells from wild-type (WT) and HSP70 knockout (KO) mice were stimulated with lipid for 24 h. The cells were immunofluorescence stained with anti-GCase antibody, and imaged under confocal microscope. The aggregation of GCase is indicated with an arrow. The numbers of aggregates of GCase were counted and indicated as aggregates/100 cells (bottom panel). (j) Binding of LIMP2 to HSP70 is also stress-induced and PGRN-dependent. Immunoprecipitation was conducted with anti-HSP70 antibody in OVA-challenged WT and PGRN KO mice, and probed with LIMP2 antibody. The result is representative of three independent experiments.

(Fig. 4c). In addition, administration of rPGRN rescued the binding of GCase to HSP70 in PGRN KO mice (Fig. 4d). HSP70 co-localized with PGRN in macrophages (Fig. 4e, f). PGRN bound to HSP70, and deletion of GrnE (i.e. CD1), known to be important for binding to GCase (Fig. 3c, g), also abolished the binding to HSP70 (Fig. 4g). We also examined whether HSP70 is required for the lysosomal localization of GCase via suppression of HSP70 using a siRNA approach. Similar to knockdown of PGRN (serving as a control), suppression of HSP70 led to a reduction of lysosomal GCase detection, assayed with the activity-based probe (ABP) MDW933, which can spontaneously cross membranes and allow sensitive and specific labeling of active lysosomal GCase in living cells (Witte et al., 2010; Gaspar et al., 2014; Aerts et al., 2011) (Fig. 4h). Further, immunofluorescence staining with anti-GCase antibody demonstrated clear aggregation of GCase in lipid-stimulated HSP70 knockout cells, but not in the WT cells (Fig. 4i), and lysotracker and MDW933 co-staining revealed elevated lysosomal storage and reduced active GCase in HSP70 KO cells as compared to control cells (Fig. S12).

Previous reports that LIMP2 is the GCase transport receptor (Reczek et al., 2007), together with the finding that both GCase and LIMP2 were aggregated in PGRN deficient macrophages (Fig. 1), led us to determine whether HSP70 also interacted with LIMP2. Similar to GCase, LIMP2 also associated with HSP70 in WT, but not in PGRN KO tissues (Fig. 4j). In addition, the interaction between LIMP2 and HSP70 is highly dependent on OVA challenge.

3.4. Development of Pcgin, a PGRN-derived Protein, Retains the Binding Activity to GCase and HSP70

The finding that PGRN acts as a co-chaperone of HSP70 and is required for disaggregation of GCase, together with the facts that chaperone-based treatments aiming to enhance GCase lysosomal localization have proven to be a promising alternative to enzyme replacement treatment (ERT) and substrate reduction therapy (SRT) for GD (Zimran et al., 2013; Sanchez-Fernandez et al., 2016; Jung et al., 2016; Mena-Barragan et al., 2015), and recombinant HSP70 has been shown to effectively correct altered lysosomal stability seen in Niemann–Pick B disease (NPD) (Kirkegaard et al., 2010), promoted us to examine whether PGRN would have therapeutic effects in GD. Indeed, we have found that recombinant PGRN protein is therapeutic against Gaucher disease (Jian et al., 2016). However, there is concern for the long-term usage of PGRN as a drug due to potential oncogenic activity of this growth factor and the established elevation of PGRN levels in various cancer tissues relative to healthy counterparts (Bateman and Bennett, 2009; He and Bateman, 1999; He et al., 2002; Zhou et al., 2015). To address this issue, we devoted considerable effort toward developing a PGRN-derived molecule that retains the GCase-binding and therapeutic activity of PGRN but lacks its oncogenic action. For this purpose, numerous PGRN mutants (i.e., C-terminal deletions, N-terminal deletions, internal deletions, and various combinations) were generated, and their interactions with GCase were tested. According to a series C-terminal and N-terminal deletion mutants, a C-terminal 98 amino acid fragment (from aa 496–593) of PGRN, containing Grn E domain, was found to be both required and sufficient for binding to GCase (Fig. 3). We next examined whether Grn E also is the functional domain that mediates PGRN's therapeutic effect against GD. Type 2 GD fibroblasts (L444P) were transfected with plasmids encoding GFP alone (negative control), PGRN-GFP and CD1-GFP (deletion of Grn E domain, Fig. 3e), and the correction of lysosomal storage was analyzed with LysoTracker Deep Red. By comparing the lysosomes in the transfected (GFP^+) and non-transfected (GFP^-) cells, we found that lysosomal storage was significantly reduced in cells expressing PGRN-GFP, compared to non-transfected cells. Interestingly, the Grn E domain is also required for PGRN-mediated therapeutic function, as the transfection of CD1-GFP, similar to the transfection with GFP empty vector, did not show any therapeutic effect (Fig. 5a, b).

To identify the "minimal fragment" that retains GCase-binding and therapeutic activity of PGRN, we dissected C-terminal 98-aa fragment with five fine-tune deletions (Fig. 5c, d). Deletion of the linker on the left, i.e. Δ496–522, the region of aa540–573 and the linker on the right of GrnE, i.e. Δ574–593, did not affect the binding to GCase and HSP70 (Fig. 5c, d), but abolished the molecule's therapeutic effects in type 2 GD fibroblasts (L444P) (Fig. 5e, f), suggesting that these regions may be needed for maintaining the proper functional conformation. However, deletion of 12 (aa523–534) and of 5 (aa535–539, RDNRQ) amino acid fragments completely abolished the binding activity to GCase and HSP70, respectively, indicating these 12 amino acids and the RDNRQ motif are responsible for binding to GCase and HSP70, respectively. Intriguingly, deletion of these critical motifs/fragments led to more severe phenotypes as compared to controls (Fig. 5e, f), suggesting that these mutants might act as the dominant negatives of endogenous PGRN. Taken together, these results suggest that the C-terminal 98 amino acid fragment appears to be the "minimal" molecule that retains GCase-binding and functional activities. This molecule was referred to as Pcgin (PGRN C-terminus for GCase Interaction). The structure and amino acid sequence of Pcgin are shown in Fig. 5g.

3.5. Pcgin Effectively Ameliorates the Phenotypes of GD

Pcgin was expressed in bacteria and purified as a His-tagged protein. The purity was examined by Coomassie Blue staining of SDS-PAGE electrophoresis gels and confirmed by Western blotting with His probe (Fig. 6a). Using a solid phase binding assay (Fig. 6b), we found that recombinant Pcgin directly bound to GCase, HSP70 and sortilin (known to bind to the last three amino acids QLL of PGRN and serving as a positive control) (Zheng et al., 2011). Although Pcgin retained the GCase and HSP70 binding activity of PGRN, it lacked PGRN's oncogenic activity, including PGRN-activated oncogenic signaling and cell proliferation (data not shown).

Since overexpression of Pcgin significantly reduced lysosomal storage in type 2 GD fibroblasts (L444P) (Fig. 5e, f), we next examined the therapeutic effects of recombinant Pcgin in GD fibroblasts. Similar to PGRN, recombinant Pcgin significantly reduced lysosomal storage content in the fibroblasts from type 2 GD L444P fibroblasts (measured by LysoTracker intensity recorded via plate reader) (Fig. 6c) and D409H fibroblasts(measured by fluorescence microscopy, followed by quantification) (Fig. 6d, e). In addition, Pcgin also effectively increased the lysosomal localization of mutant GCase (N370S) in type 1 GD fibroblasts, visualized by MDW933 labeling (Fig. 6f, g). Pcgin also reduced lysosome storage and increased lysosomal localization of mutant GCase (L444P) in type 2 GD fibroblasts (Fig. 6h). In addition, Pcgin treatment led to significant reduction in β-GlcCer storage and increase of GCase activity in type 2 GD fibroblasts (L444P) (Fig. 6i, j). We also examined Pcgin's therapeutic effect in the animal model. GD phenotype was induced by OVA challenge in 8-week-old PGRN deficient mice as described above ($n = 6$ per group). Pcgin (4 mg/kg/week) was I.P injected starting from the first week of intranasal challenge and continuing for 5 weeks, at which point, the mice were sacrificed. Another group was injected with imiglucerase as a positive control. In the untreated group, mice developed severe GD–like phenotype and large Gaucher cells occupied lung tissues. However, histology of lung tissue revealed dramatic improvement in the Pcgin treated group (Fig. 6k). Quantified data reveals that Pcgin significantly reduced number and size of Gaucher cells (Fig. 6l, m). Lipid composition analysis confirmed that Pcgin significantly reduced β-GlcCer storage as well (Fig. 6n). These results suggest that Pcgin may be a promising drug candidate in treating Gaucher disease.

4. Discussion

Recently we reported that PGRN is a previously unrecognized factor that associates with GD (Jian et al., 2016). Serum level of PGRN is significantly lower in GD patients than in healthy controls, and we have identified 4 SNP sites which may contribute to the low levels of PGRN in GD patients (Jian et al., 2016). In addition, aged PGRN null mice spontaneously develop Gaucher-like phenotypes (Jian et al., 2016). In the present study, we demonstrate that PGRN directly bound to GCase and was essential for the lysosomal appearance of GCase. In addition, HSP70, known to be crucial in unlocking protein disaggregation (Nillegoda et al., 2015; Nillegoda and Bukau, 2015), was isolated as one of numerous GCase-associated proteins dependent on the presence of PGRN in our unbiased proteomic screen. Interestingly, the interaction between GCase and HSP70, as well as their involvement in GD, had been reported previously (Lu et al., 2011; Yang et al., 2014; Ingemann and Kirkegaard, 2014), although the nature of this association was unclear. In addition, the binding of PGRN to HSP70 was also independently reported (Almeida et al., 2011). Our studies disclosed PGRN as an indispensable co-chaperone that links GCase/LIMP2 complex to HSP70. Although PGRN binds to and co-localizes with GCase in all traffic compartments, as early as the ER and Golgi apparatus, the interactions of GCase/LIMP2 with HSP70 highly depend on OVA challenge (Figs. 2, 4, Fig.

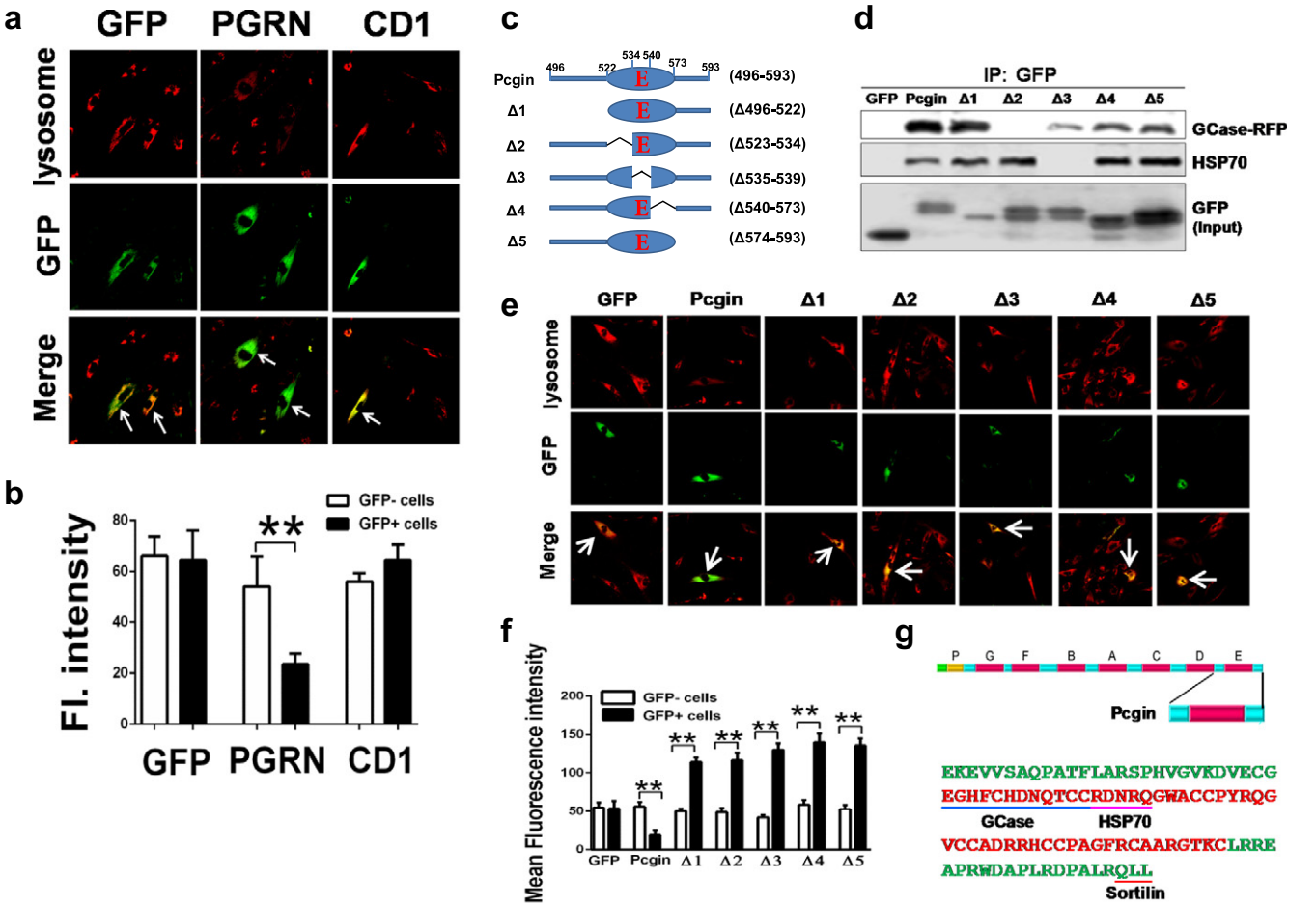

Fig. 5. Development of Pcgin. (a) Overexpression of PGRN, but not its mutant lacking Grn E, significantly reduces lysosomal storage in type 2 GD fibroblasts (L444P). GD fibroblasts were transiently transfected with plasmid encoding either GFP alone, GFP fused PGRN, or its mutant lacking GrnE (CD1-GFP), and LysoTracker® Deep Red were added after transfection, and live images were taken. Red color represents level of lysosome signal, and the green color reflects cells expressing GFP (vector) or GFP-fused proteins. Lysosomal content was compared between GFP^+ and GFP^- cells. (b) Quantification analysis of the therapeutic effects of PGRN and its mutant. Ten images were taken for each sample, and fluorescence (FL) intensity of lysosomal signals from GFP^+ and GFP^- cells were selected and quantified by Image J. The therapeutic effects were determined by comparison of the red fluorescence intensity between GFP^+ and GFP^- cells. (c) Scheme of Pcgin and its deletion mutants. (d) Co-IP assays for examining the binding of Pcgin and its mutants to GCase and HSP70. 293T cells were transfected with plasmids encoding either GFP fused Pcgin, or its mutants, together with plasmids encoding RFP fused GCase and HSP70, and the protein complexes were immunoprecipitated with GFP antibody and probed with RFP or HSP70 antibodies respectively. The bottom panel shows expression of Pcgin and its mutants in the transfected cells. The result is representative of three independent experiments. (e) Evaluation of the therapeutic effects of Pcgin and its mutations in type 2 GD fibroblasts (L444P). Fibroblasts from type 2 GD were transiently transfected with pEGFP control vector, or plasmid encoding Pcgin or its mutants. LysoTracker® Deep Red was added after transfection, and live images were taken by DV live-cell imaging system. GFP^+ cells with reduced lysosome staining exhibit a green color, while GFP^+ cells with a high level of lysosome staining give rise to a yellow color (GFP^+ cells are indicated with white arrow). (f) Quantification analysis of the therapeutic effects of Pcgin and its mutants. Ten images were taken for each sample, and fluorescence intensity of lysosomal staining from GFP^+ and GFP^- cells were quantified by Image J. The therapeutic effects were determined by comparison of the red fluorescence intensity between GFP^+ and GFP^- cells. (g) Structure and sequence of Pcgin. Pcgin is derived from C-terminal human PGRN from aa496-593, containing Grn E and linker regions on both sides (top panel). Sequence of Pcgin is shown in bottom panel. Linker regions and Grn E are highlighted in green and red, respectively. Binding sites of GCase, HSP70, and Sortilin are indicated. One-way ANOVA was used to compare means among multiple groups (Data are represented as mean ± SEM, * $p < 0.05$; ** $p < 0.01$; two sided).

S11). These results suggest that recruitment of HSP70 to the GCase/LIMP2 complex through PGRN may be stress- or disease-dependent. Under physiological conditions, GCase/LIMP2 associates with PGRN in traffic compartments, including ER/Golgi apparatus, and basal level of HSP70 may not interact or marginally interacts with this complex. Whereas under stressed or pathological conditions, such as OVA challenge, lipid stimulation and/or *GBA1* mutations, GCase/LIMP2 complex aggregates in the cytoplasm (Fig. 1f), the HSP70 disaggregation system will be recruited to GCase/LIMP2 complex through PGRN as an indispensable co-chaperone, to unlock the disaggregation of GCase/LIMP2 complex. Thus, PGRN-dependent association with HSP70 is specifically crucial for preventing the aggregation of the GCase/LIMP2 complex under pathological conditions. It is also noted that the level of HSP70 is much higher than that of PGRN (Fig. 4f), indicating that the level of PGRN may be the rate-limiting step for HSP70-mediated disaggregation of GCase/LIMP2 aggregates. Thus, it is conceivable that supplementing PGRN (Jian et al., 2016) or its derivative Pcgin may enrich or enhance the utility of HSP70, leading to the effective amelioration of GD phenotypes in various models tested (Figs. 6).

Although failing to recruit HSP70 disaggregation system to GCase/LIMP2 complex may largely account for the OVA-induced GD-like phenotype in PGRN KO mice, some known functions of PGRN may also contribute to understanding the unexpected observations in OVA-challenged PGRN KO mice. For instance, PGRN associates with TNF receptors and possesses the ability to suppress inflammation in various conditions (Zhu et al., 2002; Tang et al., 2011; Jian et al., 2013b; Liu et al., 2014; Li et al., 2014), the lack of PGRN thus likely leads to an abnormal macrophage response during OVA-induced inflammation (Fig. S1). In addition, inflammation is known to be involved in multiple sphingolipid LSDs and anti-inflammatory drugs have benefits in treating LSDs when used alone or combined with other treatments (Platt, 2014). Furthermore, PGRN has been implicated in ER-stress

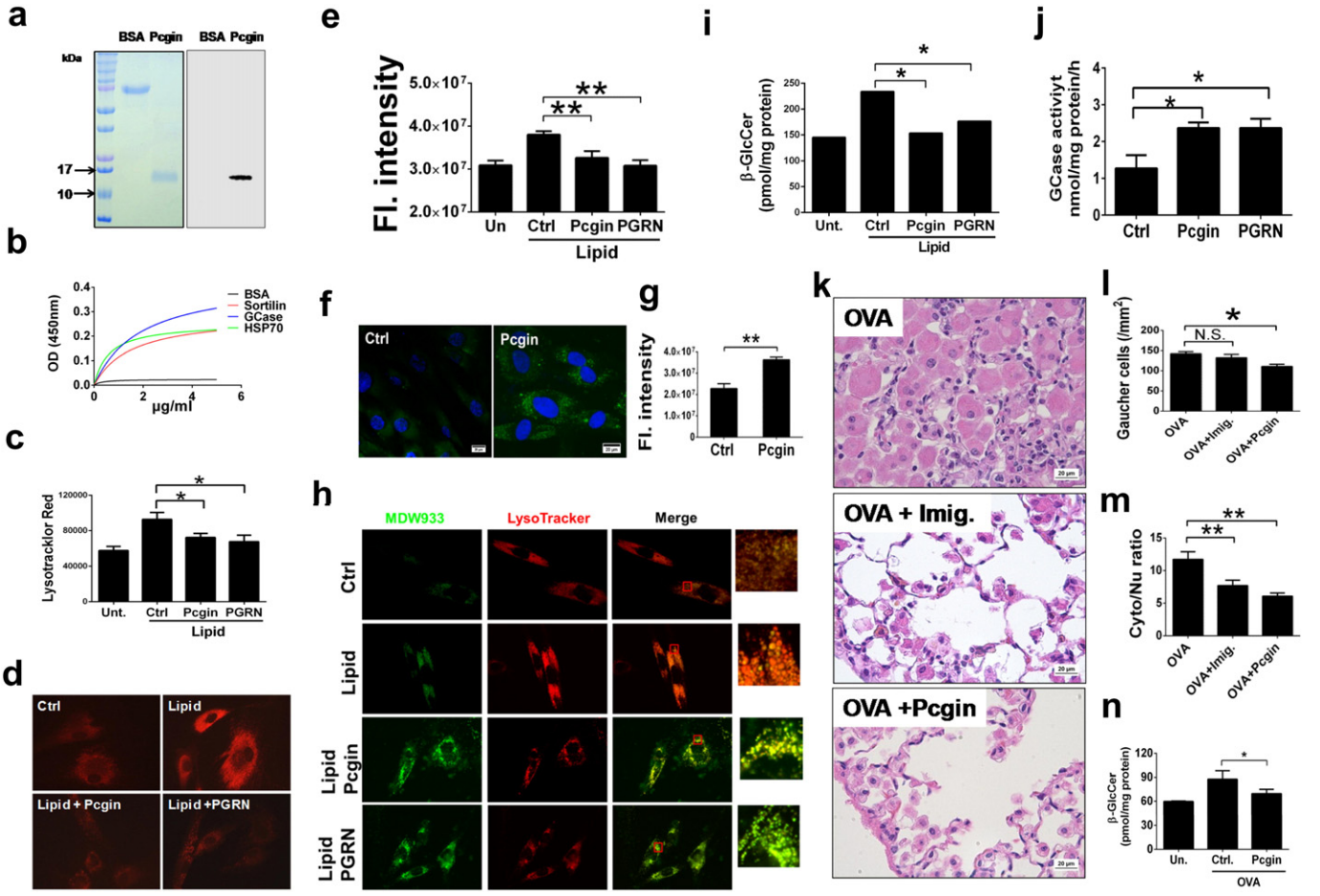

Fig. 6. Pcgin is therapeutic against GD in vitro and in vivo. (a) Expression and characterization of recombinant Pcgin. The purified Pcgin was analyzed by Coomassie blue staining (left) and Western blotting with anti-His antibody (right). (b) Recombinant Pcgin directly binds to GCase and HSP70 (Solid phase binding). Pcgin was coated on a 96-well plate and incubated with biotin-labeled GCase, HSP70, and Sortilin (serving as a positive control) respectively. Direct binding was detected by an ELISA-based method. (c) Pcgin reduces lysosomal storage as measured by lysotracker intensity. Type 2 GD fibroblasts (L444P) cultured in 96-well plates were stimulated with lipid lysis, and treated with Pcgin (5 μg/ml) or PGRN (0.4 μg/ml) for 24 h. The cells were stained with LysoTracker Red and the fluorescence intensity read using SpectraMax i3x plate reader. This data is representative of at least three independent experiments. (d) Pcgin reduces lysosomal storage in type 2 GD fibroblasts (D409H). Fibroblasts from GD patients were stimulated with lipid, or lipid plus Pcgin (5 μg/ml) and PGRN (0.4 μg/ml). Lysosomal storage was measured by LysoTracker staining. (e) Quantification of (d). Ten images per sample were taken by fluorescence microscope, and fluorescence (FL) intensity was measured by Image J software, and therapeutic effects were determined by statistical analysis. (f) Pcgin enhances lysosomal localization of mutant GCase (N370S). Type 1 GD fibroblasts were treated with Pcgin (5 μg/ml) for 24 h, and the lysosomal GCase was detected with its specific fluorescence probe MDW933. (g) Quantification of (f). Ten images per sample were taken by fluorescence microscope, and fluorescence (FL) intensity was measured by Image J software, and therapeutic effects were determined by statistical analysis. (h) Pcgin enhances lysosomal GCase and reduces lysosomal storage as measured by live imaging system. Type 2 GD fibroblasts (L444P) were cultured in a live cell imaging chamber and treated with Pcgin (5 μg/ml), or PGRN (0.4 μg/ml) for 24 h. MDW933 and LysoTracker were added and images were taken under live-cell imaging system. (i) Pcgin reduces β-GlcCer storage in GD fibroblasts. Type 2 GD fibroblasts (L444P) were stimulated with lipid lysis, along with Pcgin (5 μg/ml), or PGRN (0.4 μg/ml) treatment for 24 h. The fibroblasts were collected for β-GlcCer analysis. (j) Pcgin increases GCase activity in GD fibroblasts. Type 2 GD fibroblasts (L444P) were treated as in (i), The GCase enzymatic activity was measured. (k) Pcgin is therapeutic against GD-like phenotype in OVA-challenged PGRN KO mice. A GD-like phenotype was induced in PGRN KO mice, and mice were treated with either Pcgin or Imiglucerase (serving as a positive control) (n = 6 per group). Lung tissues were examined by H&E staining. Gaucher cell number (l) and Gaucher cell sizes (m) were significantly reduced after Pcgin treatment. (n) Pcgin reduces β-GlcCer storage in OVA-challenged PGRN KO mice. Spleens of PGRN KO mice from (k) were used to measure the levels of β-GlcCer. One-way ANOVA was used to compare means among multiple groups (Data are represented as mean ± SEM, * $p < 0.05$; ** $p < 0.01$; two sided).

related unfolded protein response (Li et al., 2014), which may play a key role in cell death in GD (Wei et al., 2008). The loss of PGRN leads to the abnormal ER stress responses and the aggregation of various proteins in the cytoplasm, such as TDP-43 (Baker et al., 2006; Tanaka et al., 2014) and GCase/LIMP2 (this paper). Recently, it was reported that RIPK3, a component of the TNFR1 signaling complex that mediates necroptosis, was also involved in the pathology of GD and inhibiting RIPK3 might be a novel therapeutic approach for GD (Vitner et al., 2014). Thus, PGRN's anti-TNF and anti-cell death activities may also contribute to its therapeutic effects in GD and other LSDs.

Many *GRN* gene mutations have been reported, and most of these mutations lead to reduced levels of PGRN (Kleinberger et al., 2013). Insufficiency of PGRN has been associated with many types of neurodegenerative diseases including FTD, Parkinson's disease (PD), Alzheimer's disease, Multiple Sclerosis, and Amyotrophic Lateral Sclerosis (Petkau and Leavitt, 2014). Our finding that PGRN is an indispensable co-chaperone of HSP70 disaggregation system required for lysosomal localization of GCase/LIMP2 may also have relevance to the pathology of neurodegenerative diseases. Mutation of the *GRN* gene may directly affect the HSP70-based disaggregases (Nillegoda and Bukau, 2015) and in turn lead to defects in the clearance of proteins associated with neurodegenerative diseases, such as TDP-43 and α-synuclein, or indirectly affect the function of lysosomes resulting from the impairment of GCase lysosomal localization and consequent accumulation of glucosylceramide (Platt et al., 2012). Thus, the identification of PGRN as a co-chaperone of HSP70 for GCase lysosomal appearance may also help us to better understand the putative molecular mechanisms underlying *GRN* mutation-associated neurodegenerative disorders. Further, heterozygosity for mutations in the *GBA1* gene may be a risk factor for PD (Eblan et al., 2005), this indicates that there may

exist a functional and a genetic linkage between *GRN* and *GBA1* genes, and that their homozygous or heterozygous mutations cause or render some carriers vulnerable to rare (i.e. GD) and/or common (i.e. PD) diseases.

Although Pcgin is a 98 amino acid c-terminal PGRN fragment, it demonstrates comparable therapeutic effects with PGRN in several types of GD patient fibroblasts bearing common *GBA1* mutations and our GD mouse model. Future investigations with additional GD models are warranted to further test the therapeutic effect and safety of Pcgin. Pcgin possesses features that suggest it may compare favorably to currently marketed GD drugs. For example, currently marketed drugs are enzyme replacement or substrate reduction therapies. In contrast, Pcgin functions as a co-chaperone of HSP70 and enhances the disaggregation and lysosomal appearance of mutant lysosomal enzymes. Due to this alternate mechanism of action, Pcgin may be effective for other LSDs in addition to GD. Additionally, Pcgin's safety (lacking PGRN's potential oncogenic activity) and ease of production (as a small ~15 kD recombinant protein) suggest that it may be a viable cost-effective agent for the clinical treatment of LSDs, in particular GD.

In summary, this study identifies PGRN as a previously-unrecognized molecule associated with GCase, thus providing a foundation for future discoveries relating to this critical factor in GD and other lysosomal storage diseases. In addition, it also isolates PGRN as a co-chaperone of HSP70 disaggregation system, thus uncovering a unique strategy to target this cardinal pathway of metabolic diseases. More importantly, we have developed a PGRN derivative, Pcgin, which effectively ameliorates the phenotypes of GD in several preclinical models. With the consideration that HSP70 is involved in a plethora of disease processes, the identification and manipulation of this new co-chaperone of HSP70 may lead to innovative therapeutics for LSDs, in particular GD, and other metabolic pathologies and conditions.

Author Contributions

J. Jian designed and performed experiments, collected and analyzed data, and wrote the paper. Q.Y. Tian, A. Hettinghouse, S. Zhao, H. Liu, and J. Wei performed experiments, collected and analyzed data. G. Grunig established the chronic lung inflammation model, collected and analyzed data. W. Zhang, K. Setchell, and Y. Sun. performed lipid analysis and edited manuscript. H. S. Overkleeft contributed new reagents/analytic tools. G. L. Chan participated the experimental design and data analysis. C. J. Liu designed and supervised this study, analyzed data, and wrote and edited the manuscript. All authors contributed discussions and interpretations of the data.

Acknowledgements

We thank Yi Zhang, Peiying Shan and Petty Lee at Yale University for providing murine lung endothelial cells isolated from wild-type and HSP70$^{-/-}$ mice, David Goad and Aaron Martin at SensiQ Technologies, Inc. (Oklahoma City, OK 73104) for Surface Plasmon Resonance (SPR) assay with SensíQ Pioneer, and Fengxia Liang, Yan Deng, Chris Petzold and Kristen Dancel at NYU Medical School OCS Microscopy Core for their assistance with electronic microscope image, Venette Inskeep at Cincinnati Children's Hospital Medical Center for technical support in lipid analysis.

This work was supported partly by NIH research grants R01AR062207, R01AR061484, and a research grant from Atreaon (to C. J. Liu).

All authors disclose no conflict of interests.

Patents have been filed by NYU that claim PGRN and its derivatives for diagnosis and treatment of Gaucher disease and other lysosomal storage diseases (Docket No. 1049-1-224P).

Appendix A. Supplementary data

Supplementary data to this article can be found online at http://dx.doi.org/10.1016/j.ebiom.2016.10.010.

References

Aerts, J.M., et al., 2011. Biomarkers in the diagnosis of lysosomal storage disorders: proteins, lipids, and inhibodies. J. Inherit. Metab. Dis. 34, 605–619. http://dx.doi.org/10.1007/s10545-011-9308-6.

Ahmed, Z., et al., 2010. Accelerated lipofuscinosis and ubiquitination in granulin knockout mice suggest a role for progranulin in successful aging. Am. J. Pathol. 177, 311–324. http://dx.doi.org/10.2353/ajpath.2010.090915.

Almeida, S., Zhou, L., Gao, F.B., 2011. Progranulin, a glycoprotein deficient in frontotemporal dementia, is a novel substrate of several protein disulfide isomerase family proteins. PLoS One 6, e26454. http://dx.doi.org/10.1371/journal.pone.0026454.

Baker, M., et al., 2006. Mutations in progranulin cause tau-negative frontotemporal dementia linked to chromosome 17. Nature 442, 916–919. http://dx.doi.org/10.1038/nature05016.

Bateman, A., Bennett, H.P., 2009. The granulin gene family: from cancer to dementia. Bioessays 31, 1245–1254. http://dx.doi.org/10.1002/bies.200900086.

Beutler, E., 1991. Gaucher's disease. N. Engl. J. Med. 325, 1354–1360. http://dx.doi.org/10.1056/NEJM199111073251906.

Brady, R.O., Kanfer, J.N., Shapiro, D., 1965. Metabolism of glucocerebrosides. II. Evidence of an enzymatic deficiency in Gaucher's disease. Biochem. Biophys. Res. Commun. 18, 221–225.

Cruts, M., et al., 2006. Null mutations in progranulin cause ubiquitin-positive frontotemporal dementia linked to chromosome 17q21. Nature 442, 920–924. http://dx.doi.org/10.1038/nature05017.

Daley, E., et al., 2008. Pulmonary arterial remodeling induced by a Th2 immune response. J. Exp. Med. 205, 361–372. http://dx.doi.org/10.1084/jem.20071008.

de la Mata, M., et al., 2015. Pharmacological chaperones and coenzyme Q10 treatment improves mutant beta-glucocerebrosidase activity and mitochondrial function in neuronopathic forms of Gaucher disease. Sci. Rep. 5, 10903. http://dx.doi.org/10.1038/srep10903.

Eblan, M.J., Walker, J.M., Sidransky, E., 2005. The glucocerebrosidase gene and Parkinson's disease in Ashkenazi Jews. N. Engl. J. Med. 352, 728–731. http://dx.doi.org/10.1056/NEJM200502173520719.

Feng, J.Q., Guo, F.J., Jiang, B.C., Zhang, Y., Frenkel, S., Wang, D.W., Tang, W., Xie, Y., Liu, C.J., 2010. Granulin epithelin precursor: a bone morphogenic protein 2-inducible growth factor that activates Erk1/2 signaling and JunB transcription factor in chondrogenesis. FASEB J 24 (6), 1879–1892. http://dx.doi.org/10.1096/fj.09-144659.

Gaspar, P., et al., 2014. Action myoclonus-renal failure syndrome: diagnostic applications of activity-based probes and lipid analysis. J. Lipid Res. 55, 138–145. http://dx.doi.org/10.1194/jlr.M043802.

Gegg, M.E., Schapira, A.H., 2016. Mitochondrial dysfunction associated with glucocerebrosidase deficiency. Neurobiol. Dis. 90, 43–50. http://dx.doi.org/10.1016/j.nbd.2015.09.006.

Gonzalez, E.M., Mongiat, M., Slater, S.J., Baffa, R., Iozzo, R.V., 2003. A novel interaction between perlecan protein core and progranulin: potential effects on tumor growth. J. Biol. Chem. 278, 38113–38116. http://dx.doi.org/10.1074/jbc.C300310200.

Gotzl, J.K., et al., 2014. Common pathobiochemical hallmarks of progranulin-associated frontotemporal lobar degeneration and neuronal ceroid lipofuscinosis. Acta Neuropathol. 127, 845–860. http://dx.doi.org/10.1007/s00401-014-1262-6.

Grabowski, G.A., 2012. Gaucher disease and other storage disorders. Hematology/the Education Program of the American Society of Hematology 2012. American Society of Hematology. Education Program, pp. 13–18. http://dx.doi.org/10.1182/asheducation-2012.1.13.

He, Z., Bateman, A., 1999. Progranulin gene expression regulates epithelial cell growth and promotes tumor growth in vivo. Cancer Res. 59, 3222–3229.

He, Z., Ismail, A., Kriazhev, L., Sadvakassova, G., Bateman, A., 2002. Progranulin (PC-cell-derived growth factor/acrogranin) regulates invasion and cell survival. Cancer Res. 62, 5590–5596.

He, Z., Ong, C.H., Halper, J., Bateman, A., 2003. Progranulin is a mediator of the wound response. Nat. Med. 9, 225–229. http://dx.doi.org/10.1038/nm816.

Hrabal, R., Chen, Z., James, S., Bennett, H.P., Ni, F., 1996. The hairpin stack fold, a novel protein architecture for a new family of protein growth factors. Nat. Struct. Biol. 3, 747–752.

Ingemann, L., Kirkegaard, T., 2014. Lysosomal storage diseases and the heat shock response: convergences and therapeutic opportunities. J. Lipid Res. 55, 2198–2210. http://dx.doi.org/10.1194/jlr.R048090.

Jian, J., Konopka, J., Liu, C., 2013a. Insights into the role of progranulin in immunity, infection, and inflammation. J. Leukoc. Biol. 93, 199–208. http://dx.doi.org/10.1189/jlb.0812429.

Jian, J., et al., 2013b. Progranulin directly binds to the CRD2 and CRD3 of TNFR extracellular domains. FEBS Lett. 587, 3428–3436. http://dx.doi.org/10.1016/j.febslet.2013.09.024.

Jian, J., et al., 2016. Association Between Progranulin and Gaucher's Disease. EBioMedicine http://dx.doi.org/10.1016/j.ebiom.2016.08.004.

Jung, O., Patnaik, S., Marugan, J., Sidransky, E., Westbroek, W., 2016. Progress and potential of non-inhibitory small molecule chaperones for the treatment of Gaucher disease

and its implications for Parkinson disease. Expert Rev. Proteomics 13, 471–479. http://dx.doi.org/10.1080/14789450.2016.1174583.
Kirkegaard, T., et al., 2010. Hsp70 stabilizes lysosomes and reverts Niemann-Pick disease-associated lysosomal pathology. Nature 463, 549–553. http://dx.doi.org/10.1038/nature08710.
Kleinberger, G., Capell, A., Haass, C., Van Broeckhoven, C., 2013. Mechanisms of granulin deficiency: lessons from cellular and animal models. Mol. Neurobiol. 47, 337–360. http://dx.doi.org/10.1007/s12035-012-8380-8.
Li, M., et al., 2014. Progranulin is required for proper ER stress response and inhibits ER stress-mediated apoptosis through TNFR2. Cell. Signal. 26, 1539–1548. http://dx.doi.org/10.1016/j.cellsig.2014.03.026.
Liu, C., Li, X.X., Gao, W., Liu, W., Liu, D.S., 2014. Progranulin-derived Atsttrin directly binds to TNFRSF25 (DR3) and inhibits TNF-like ligand 1A (TL1A) activity. PLoS One 9, e92743. http://dx.doi.org/10.1371/journal.pone.0092743.
Lu, J., et al., 2011. Histone deacetylase inhibitors prevent the degradation and restore the activity of glucocerebrosidase in Gaucher disease. Proc. Natl. Acad. Sci. U. S. A. 108, 21200–21205. http://dx.doi.org/10.1073/pnas.1119181109.
Matsuda, J., et al., 2003. Chemical chaperone therapy for brain pathology in G(M1)-gangliosidosis. Proc. Natl. Acad. Sci. U. S. A. 100, 15912–15917. http://dx.doi.org/10.1073/pnas.2536657100.
Mena-Barragan, T., et al., 2015. pH-responsive pharmacological chaperones for rescuing mutant Glycosidases. Angew. Chem. Int. Ed. Eng. 54, 11696–11700. http://dx.doi.org/10.1002/anie.201505147.
Nillegoda, N.B., Bukau, B., 2015. Metazoan Hsp70-based protein disaggregases: emergence and mechanisms. Front. Mol. Biosci. 2, 57. http://dx.doi.org/10.3389/fmolb.2015.00057.
Nillegoda, N.B., et al., 2015. Crucial HSP70 co-chaperone complex unlocks metazoan protein disaggregation. Nature 524, 247–251. http://dx.doi.org/10.1038/nature14884.
Parenti, G., Andria, G., Valenzano, K.J., 2015. Pharmacological chaperone therapy: preclinical development, clinical translation, and prospects for the treatment of lysosomal storage disorders. Mol. Ther. 23, 1138–1148. http://dx.doi.org/10.1038/mt.2015.62.
Park, S.H., et al., 2015. The effects of antigen-specific IgG1 antibody for the pulmonary-hypertension-phenotype and B cells for inflammation in mice exposed to antigen and fine particles from air pollution. PLoS One 10, e0129910. http://dx.doi.org/10.1371/journal.pone.0129910.
Petkau, T.L., Leavitt, B.R., 2014. Progranulin in neurodegenerative disease. Trends Neurosci. 37, 388–398. http://dx.doi.org/10.1016/j.tins.2014.04.003.
Platt, F.M., 2014. Sphingolipid lysosomal storage disorders. Nature 510, 68–75. http://dx.doi.org/10.1038/nature13476.
Platt, F.M., Boland, B., van der Spoel, A.C., 2012. The cell biology of disease: lysosomal storage disorders: the cellular impact of lysosomal dysfunction. J. Cell Biol. 199, 723–734. http://dx.doi.org/10.1083/jcb.201208152.
Reczek, D., et al., 2007. LIMP-2 is a receptor for lysosomal mannose-6-phosphate-independent targeting of beta-glucocerebrosidase. Cell 131, 770–783. http://dx.doi.org/10.1016/j.cell.2007.10.018.
Rothman, J.E., Schekman, R., 2011. Molecular mechanism of protein folding in the cell. Cell 146, 851–854. http://dx.doi.org/10.1016/j.cell.2011.08.041.
Sanchez-Fernandez, E.M., Garcia Fernandez, J.M., Mellet, C.O., 2016. Glycomimetic-based pharmacological chaperones for lysosomal storage disorders: lessons from Gaucher, GM1-gangliosidosis and Fabry diseases. Chem. Commun. (Camb.) 52, 5497–5515. http://dx.doi.org/10.1039/c6cc01564f.
Sun, Y., Quinn, B., Witte, D.P., Grabowski, G.A., 2005. Gaucher disease mouse models: point mutations at the acid beta-glucosidase locus combined with low-level prosaposin expression lead to disease variants. J. Lipid Res. 46, 2102–2113. http://dx.doi.org/10.1194/jlr.M500202-JLR200.
Tanaka, Y., Chambers, J.K., Matsuwaki, T., Yamanouchi, K., Nishihara, M., 2014. Possible involvement of lysosomal dysfunction in pathological changes of the brain in aged progranulin-deficient mice. Acta Neuropathol. Commun. 2, 78. http://dx.doi.org/10.1186/s40478-014-0078-x.
Tang, W., et al., 2011. The growth factor progranulin binds to TNF receptors and is therapeutic against inflammatory arthritis in mice. Science 332, 478–484. http://dx.doi.org/10.1126/science.1199214.
Thurner, L., et al., 2013. Progranulin antibodies entertain a proinflammatory environment in a subgroup of patients with psoriatic arthritis. Arthritis Res. Ther. 15, R211. http://dx.doi.org/10.1186/ar4406.
Thurner, L., et al., 2014. Proinflammatory progranulin antibodies in inflammatory bowel diseases. Dig. Dis. Sci. 59, 1733–1742. http://dx.doi.org/10.1007/s10620-014-3089-3.
Vitner, E.B., et al., 2014. RIPK3 as a potential therapeutic target for Gaucher's disease. Nat. Med. 20, 204–208. http://dx.doi.org/10.1038/nm.3449.
Wei, H., et al., 2008. ER and oxidative stresses are common mediators of apoptosis in both neurodegenerative and non-neurodegenerative lysosomal storage disorders and are alleviated by chemical chaperones. Hum. Mol. Genet. 17, 469–477. http://dx.doi.org/10.1093/hmg/ddm324.
Witte, M.D., et al., 2010. Ultrasensitive in situ visualization of active glucocerebrosidase molecules. Nat. Chem. Biol. 6, 907–913. http://dx.doi.org/10.1038/nchembio.466.
Yang, C., et al., 2014. Celastrol increases glucocerebrosidase activity in Gaucher disease by modulating molecular chaperones. Proc. Natl. Acad. Sci. U. S. A. 111, 249–254. http://dx.doi.org/10.1073/pnas.1321341111.
Zhang, Y.I., et al., 2016. An endothelial Hsp70-TLR4 axis limits Nox3 expression and protects against oxidant injury in lungs. Antioxid. Redox Signal. http://dx.doi.org/10.1089/ars.2015.6505.
Zheng, Y., Brady, O.A., Meng, P.S., Mao, Y., Hu, F., 2011. C-terminus of progranulin interacts with the beta-propeller region of sortilin to regulate progranulin trafficking. PLoS One 6, e21023. http://dx.doi.org/10.1371/journal.pone.0021023.
Zhou, B., et al., 2015. Progranulin induces adipose insulin resistance and autophagic imbalance via TNFR1 in mice. J. Mol. Endocrinol. 55, 231–243. http://dx.doi.org/10.1530/JME-15-0075.
Zhu, J., et al., 2002. Conversion of proepithelin to epithelins: roles of SLPI and elastase in host defense and wound repair. Cell 111, 867–878.
Zimran, A., Altarescu, G., Elstein, D., 2013. Pilot study using ambroxol as a pharmacological chaperone in type 1 Gaucher disease. Blood Cells Mol. Dis. 50, 134–137. http://dx.doi.org/10.1016/j.bcmd.2012.09.006.